Ocular Changes in TgF344-AD Rat Model of Alzheimer's Disease

Yuchun Tsai,[1] Bin Lu,[1] Alexander V. Ljubimov,[1,2] Sergey Girman,[1] Fred N. Ross-Cisneros,[3] Alfredo A. Sadun,[3] Clive N. Svendsen,[1,2] Robert M. Cohen,[4] and Shaomei Wang[1]

[1]Cedars-Sinai Regenerative Medicine Institute, Los Angeles, California
[2]David Geffen School of Medicine at UCLA, Los Angeles, California
[3]Doheny Eye Institute and Department of Ophthalmology, Keck School of Medicine, University of Southern California, Los Angeles, California
[4]Emory University, Department of Psychiatry and Behavioral Sciences, Atlanta, Georgia

Correspondence: Shaomei Wang, Regenerative Medicine Institute, Cedars-Sinai Medical Center, 8700 Beverly Boulevard, AHSP-8107, Los Angeles, CA 90048; shaomei.wang@cshs.org.

Submitted: July 22, 2013
Accepted: December 17, 2013

Citation: Tsai Y, Lu B, Ljubimov AV, et al. Ocular changes in TgF344-AD rat model of Alzheimer's disease. *Invest Ophthalmol Vis Sci*. 2014;55:523–534. DOI:10.1167/iovs.13-12888

Purpose. Alzheimer's disease (AD) is the most common neurodegenerative disorder characterized by progressive decline in learning, memory, and executive functions. In addition to cognitive and behavioral deficits, vision disturbances have been reported in early stage of AD, well before the diagnosis is clearly established. To further investigate ocular abnormalities, a novel AD transgenic rat model was analyzed.

Methods. Transgenic (Tg) rats (TgF344-AD) heterozygous for human mutant APPswe/PS1ΔE9 and age-matched wild type (WT) rats, as well as 20 human postmortem retinal samples from both AD and healthy donors were used. Visual function in the rodent was analyzed using the optokinetic response and luminance threshold recording from the superior colliculus. Immunohistochemistry on retinal and brain sections was used to detect various markers including amyloid-β (Aβ) plaques.

Results. As expected, Aβ plaques were detected in the hippocampus, cortex, and retina of Tg rats. Plaque-like structures were also found in two AD human whole-mount retinas. The choroidal thickness was significantly reduced in both Tg rat and in AD human eyes when compared with age-matched controls. Tg rat eyes also showed hypertrophic retinal pigment epithelial cells, inflammatory cells, and upregulation of complement factor C3. Although visual acuity was lower in Tg than in WT rats, there was no significant difference in the retinal ganglion cell number and retinal vasculature.

Conclusions. In this study, we observed pathological changes in the choroid and in RPE cells in the TgF344-AD rat model; choroidal thinning was observed further in human AD retina. Along with Aβ deposition, the inflammatory response was manifested by microglial recruitment and complement activation. Further studies are needed to elucidate the significance and mechanisms of these pathological changes.

Keywords: Alzheimer's disease, choroidal thickness, visual acuity, retinal pigment epithelium

Alzheimer's disease (AD) is the leading cause of dementia, which is characterized by loss of memory and a progressive decline in cognitive function. To date, over 26 million people are estimated to suffer from AD, and the number is expected to quadruple by 2050.[1] The characteristic lesions in AD are amyloid-β (Aβ) plaque deposition, formation of neurofibrillary tangles (NFTs), neuronal loss, and inflammation, all of which lead to degeneration of neurons and synapses in the brain.[2] Although AD has been described over a century ago, treatment and understanding of the pathogenesis are still rather limited.[2]

In addition to cognitive abnormalities, visual symptoms have been reported in early stages of AD even before the diagnosis is clearly established.[3,4] Visual examinations in patients with AD have revealed anomalies in visual acuity,[4] contrast sensitivity,[5] color vision,[6] and motion perception.[7] Armstrong et al.[8] suggested that senile plaques and NFTs are dominant in the cuneal gyrus, which is consistent with the inferior field defects in AD.[9] However, whether visual problems in AD are related to cortical disease or retinal abnormalities remains controversial. Indeed, increasing evidence indicates that retinal changes such as degeneration and loss of retinal ganglion cells (RGC),[10–12] reduction of the retinal nerve fiber layer (RNFL) thickness,[13–15] and reduced retinal blood flow[16] may partially account for visual dysfunctions[17] in AD patients, as in those affected with some other neurodegenerative diseases, including demyelinating optic neuritis, multiple sclerosis, and Parkinson disease.[18]

Recently, the pathogenesis of AD has been focused on cerebral vasculature and the manifestations in the choroid plexus (CP), in connection with the deficient clearance of Aβ across the blood-brain barrier[19,20] and the blood-cerebrospinal fluid (CSF) barrier.[21,22] Atrophy of epithelial cells leads to CP abnormalities and alteration of synthesis, secretion and transportation of proteins. As the eye and the brain share many features in terms of embryological origin, anatomical, and physiological characteristics,[18] investigating the changes of ocular vasculature in AD might shed light on the pathological mechanisms.

In the past decade, transgenic (Tg) mouse models overexpressing mutant forms of amyloid precursor protein (APP) and/or presenilin 1 (PS1) have been generated to mimic various aspects of AD pathology, including Aβ deposition, cognitive

Copyright 2014 The Association for Research in Vision and Ophthalmology, Inc.

Table 1. List of Antibodies Used in the Study

Name	Dilution	Manufacturer
Mouse anti-amyloid-β (6E10)	1:500	Covance
Mouse anti-RPE65	1:1000	Millipore
Rabbit anti-type IV collagen*	1:1000	Millipore
Mouse anti-Iba-1	1:500	Abcam
Goat anti-CD68	1:300	Abcam
Rabbit anti-C3 complement	1:300	Santa Cruz
Mouse anti-GFAP	1:500	Sigma
Mouse anti-RT97	1:1000	Millipore
FITC-conjugated goat anti-mouse IgG	1:300	Dianova
Cy3-conjugated donkey anti-goat IgG	1:300	Dianova
AlexaFluor 568-conjugated donkey anti-rabbit IgG	1:500	Life Technologies

* The antibody is supposed to react with α1/α2 type IV collagen isoform, as the antigen was purified from EHS tumor matrix that does not contain α3(IV)-α5(IV) chains.[93] This is the major isoform in choriocapillaris and Bruch's membrane.[94]

deficits, inflammation, and synaptic dysfunction.[23] Likewise, several studies have shown the Aβ deposits in the retina[24] and retinal vasculature,[25] loss of retinal ganglion cells,[25] and activated glial cells[25,26] in different strains of Tg animals. Nevertheless, none of these mouse models faithfully recapitulate the pathology of AD patients. Here, we examined the changes in the eye using a novel Tg AD rat model, TgF344-AD, which has a healthy long lifespan but suffers cognitive decline at later ages, age-dependent cerebral amyloidosis, taupathy, gliosis, and neuronal loss that parallel those in humans.[27] Deposition of Aβ plaques in both brains and eyes, reduction of choroidal thickness, hypertrophy of RPE cells and inflammatory response in choroid are described here in the Tg rats. Importantly, the reduction of choroidal thickness was observed in retinas of postmortem eyes from AD patients, although using a limited sample size.

Materials and Methods

Transgenic Rats

We used 19-month-old Tg rats (of both males and females) and age-matched WT controls for visual function tests. At least eight eyes were examined in each group. For histological analysis, 14- and 19-month-old rats were used and at least 12 eyes were analyzed in each group. The heterozygous TgF344-AD rats on a Fischer-344 background used in this study coexpress human APP 695 with mutations (K595N, M596L), and PS1 with deletion of exon 9. The Tg rats were generated by pronuclear coinjection of two plasmids, MoPrP-APPswe and MoPrp-PS1ΔE9, which has a separate mouse prion promoter. The animals were housed and maintained at the Cedars-Sinai Medical Center, Department of Comparative Medicine vivarium. All animal protocols were approved by the Institutional Animal Care and Use Committee (IACUC).

Visual Functional Analysis

Visual acuity was tested by optokinetic response (OKR) on both Tg and WT rats according to our published protocol.[28] Luminance threshold recordings from the superior colliculus (SC) were obtained using our previous protocol.[29]

Light Microscopical Immunohistochemistry

Rats were euthanized with CO_2 and transcardially perfused with 4% paraformaldehyde in PBS, followed by postfixation of the eyes and brains in the same fixative for 1 hour and overnight, respectively. Tissues were cryoprotected in PBS with 30% sucrose overnight at 4°C. Samples were then embedded in OCT and cut into 10-μm sections on a cryostat (Leica CM1850; Leica Microsystems, Wetzlar, Germany). The sections were collected according to our previous protocol.[30] One slide from each set was stained with cresyl violet (CV) to assess integrity of retinal lamination; the rest of the slides stored at −40°C were used for immunohistochemistry. The same protocol was applied for brain sections, but section thickness was 30 μm. For Aβ plaque staining, sections were blocked with 5% horse serum (HS) with 0.25% Triton X-100 for 1 hour at room temperature and incubated overnight at 4°C with the primary 6E10 anti-Aβ antibody. For controls, retinal sections were processed as above, but without primary antibody or with diaminobenzidine (DAB) only. Retinal sections were then incubated with the secondary antibody coupled with biotin for 1 hour at room temperature followed by avidin–biotin enhancer complex coupled with HRP (ABC Elite; Vector Laboratories, Burlingame, CA) for 1 hour at room temperature. After 30 minutes of washing with PBS, DAB (Vector Laboratories) was added and the reaction was stopped in distilled water after 5 minutes of washing. Slides were lightly counterstained with CV, dehydrated, mounted using CV mount medium, and examined by regular light microscopy.

Immunofluorescence and Confocal Microscopic Imaging

Retinal sections were permeabilized and blocked with 10% HS with 0.25% Triton X-100 for 1 hour at room temperature and then incubated with primary antibodies or PBS as control overnight at 4°C followed by secondary antibodies for 1 hour at room temperature, with DAPI nuclear counterstaining. Primary and secondary antibodies used in this study are listed in Table 1. Retinal sections were mounted with fluorescent mounting medium (DAKO, Carpinteria, CA) for imaging. Images were taken with a confocal microscope (Eclipse C1si; Nikon Instruments, Inc., Melville, NY) and a fluorescence microscope (Olympus BTX40; Olympus America, Inc., Center Valley, PA).

Retrograde Labeling With Neuronal Tracer and Retinal Whole Mount Preparation

To quantify the number of RGC, a neuronal tracer (Fluoro-Gold; Fluorochrome, LLC, Denver, CO) was applied to the SC as described.[31] Briefly, the animals were anesthetized, placed into a stereotactic apparatus, and the skull was cut. A small piece of gelatin sponge soaked in 3% neuronal tracer (Fluorochrome, LLC) was laid over the center of SC, and a retinal whole mount was prepared 5 days after surgery as follows. Animals were perfused with PBS, followed by 4% paraformaldehyde. The orientation of the eye was marked. The eyes were flattened by four radial cuts and the entire retina was removed under the dissecting microscope. The retina was postfixed for 30 minutes in the same fixative and infiltrated in 30% sucrose at 4°C. Before blocking, the whole mount retina was frozen at −80°C for 15 minutes to assist antibody penetration, followed by immunofluorescent staining as described above.

Quantification

To measure the thickness of choroid in the retinal sections, at least seven retinal sections from each animal cut in the same horizontal angle across optic nerve were stained with type IV collagen antibody and the fluorescence signal was measured by Java-based image processing software version 1.46 (ImageJ; National Institutes of Health [NIH], Bethesda, MD). The

Investigative Ophthalmology & Visual Science

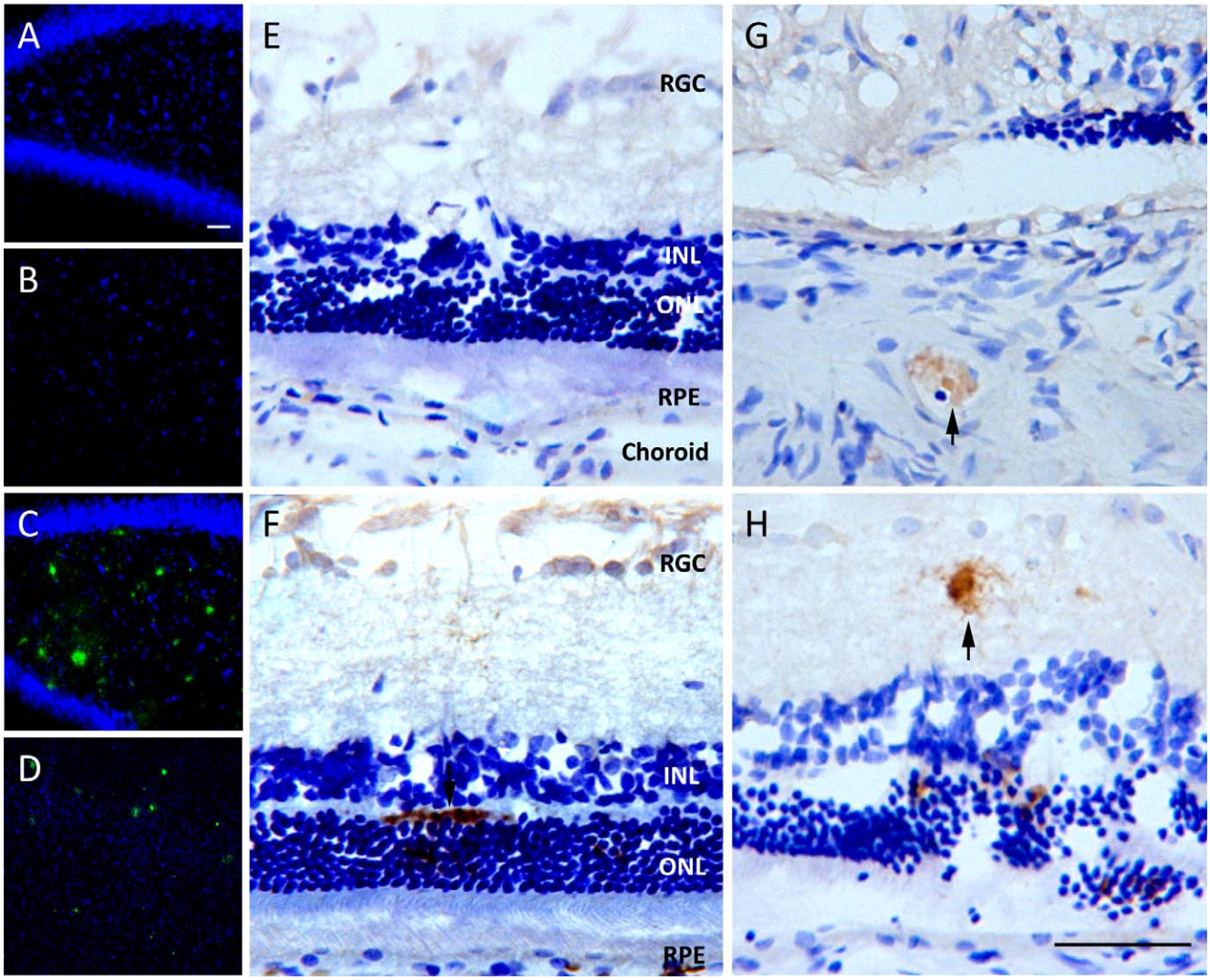

Figure 1. Aβ immunoreactivity in 19-months WT and TgF344-AD rats. Immunofluorescent staining with 6E10 antibody did not show any signal in the WT (**A**, **B**), but robust and variable-sized Aβ plaques in Tg rat brain (**C**, **D**). Both hippocampus (**A**, **C**) and cortex (**B**, **D**) were examined. Immunoreactivity (DAB) for Aβ in WT (**E**) and Tg (**F**–**H**) retinal sections. Aβ plaques were found in the OPL (**F**), choroid (**G**), and IPL ([**H**]; *arrows*). ONL: outer nuclear layer. *Scale bars*: 50 μm.

thickness of the retinal choroid was measured according to the published protocol[32] and rat sections were collected as we previously described.[30] Briefly, four cryostat sections (50 μm apart) were collected per slide providing five 1 in 4 series. One series was stained with CV for assessing integrity of retinal lamination, the rest was stained for antibodies. Approximately 80 slides were generated per eye with one series of 16 slides. The thickness of the choroid was defined as the distance between the outer border of the Bruch's membrane and the inner border of the sclera. Measurements were performed by Java-based image processing software version 1.6 (NIH). The values for each eye were averaged and the statistical analysis was performed. The total numbers of Iba-1 positive cells (microglia) in the choroid were assessed for every 10th retinal section in the WT and Tg animals. At least five eyes were examined in WT and Tg rats, respectively. Counting of RGCs was adapted from the previously published procedure for the rat retina.[33] Briefly, images of six standard rectangular areas from the optic disc in the central regions of each retinal quadrant were captured. All neuronal tracer–labeled (Fluorochrome, LLC) RGCs were counted using a cell-counter plugin based on Java-based imaging software (NIH). The total number of RGCs was summed up and statistical analysis was performed between WT and Tg groups.

Human Autopsy Specimens

Human postmortem control eyes were received from the Lions Vision Gift eye bank in Portland, Oregon, and the AD eyes were acquired through the Alzheimer's Disease Research Center (ADRC) Neuropathology Core at the University of Southern California (USC) or National Disease Research Interchange (NDRI, Philadelphia, PA). The ADRC at USC is funded by the National Institute of Aging. The acquisition of donor tissue through the ADRC at USC has been approved by an Institutional Review Board (IRB) at USC. The Lions Vision Gift eye bank enucleates from the anterior aspect of the orbit and the ADRC from the posterior side. Prior to enucleation, both the Lions Vision Gift eye bank and ADRC initially dissect away the conjunctiva, extraocular muscles, and surrounding connective tissues and minor nerves. Then both groups enucleate the eyes by cutting away the optic nerves and gently extracting the tissues from the orbit anteriorly or posteriorly. The

Investigative Ophthalmology & Visual Science

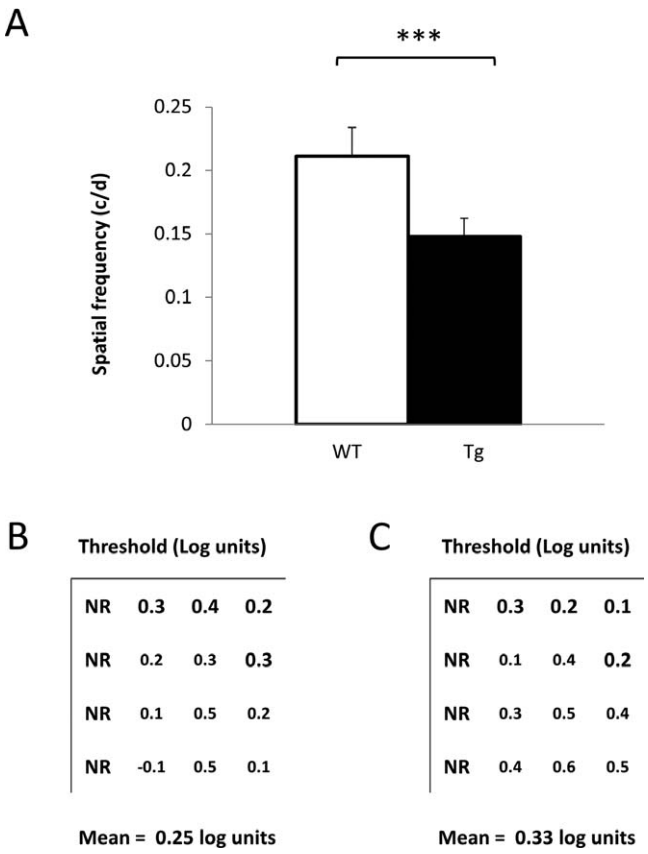

FIGURE 2. Visual dysfunction in TgF344-AD rats. (**A**) Spatial visual acuity was recorded using Optometry head tracking apparatus. In 19-month-old Tg rats, spatial visual acuity was significantly declined compared with age-matched WT rats (mean ± SEM, $n = 8$. *** $P \leq 0.01$). To measure retinal sensitivity to light across the visual field, a single and multiunit activities of luminance threshold responses were recorded at 16 points within the SC from 19-month-old WT (**B**) and Tg (**C**) rats. Although retinal sensitivities in Tg rats were reduced compared with WT rats, uneven luminance thresholds across the superior colliculus were observed in both Tg and control rats.

posterior extraction of the eye performed by the ADRC occurs after the removal of the brain. Furthermore, both tissue banks immersion fix the eyes in neutral buffered formalin, and all tissues are dissected, processed, embedded into paraffin, and sectioned by the same laboratory. NDRI supplied nonfixed eyes in corneal storage medium (Optisol-GS, Chiron IntraOptics, Irvine, CA). Six patients with AD (aged 63, 64, 75, 80, 80, and 95 years) and six age-matched control subjects (aged 64, 76, 80, 85, 93, and 95 years) at autopsy (postmortem interval 3–13 hours) were analyzed. The diagnosis of AD was confirmed clinicopathologically in accordance with modified Consortium to Establish a Registry for Alzheimer's Disease (CERAD) or National Institute on Aging (NIA)-Reagan criteria and Braak–Braak Alzheimer classification.[34,35] Age-matched eyes that were from patients not having a diagnosis of AD served as control specimens in the study. Neither the patients with AD nor the patients from whom the control tissues were obtained had any history of diabetes mellitus, metastatic cancers, ocular diseases, or sepsis. Eyes were immersion-fixed in 10% neutral buffered formalin immediately following enucleation. Eyes were dissected at the horizontal meridian through the optic nerve and nasal and temporal regions of the retina. Tissues were then processed for paraffin embedding, cut at 5 μm on a retracting microtome, and prepared for immunohistochemistry. After dewaxing in xylene, rehydrating in decreasing grades of ethanol, and antigen retrieval, the same antibodies used for rat tissues targeting epitopes for type IV collagen, RPE65, and Aβ (6E10) were also used for human tissues. The thickness of choroid was measured using the same method as described above for the rat tissues. Four fresh eyes from AD donors (age: 79 and 79 years) and four fresh eyes from normal controls (age: 78 and 83 years) were prepared for whole-mount staining with Thioflavin-T according to protocol described by Picket and Herrera,[36] and Aβ (6E10) antibody using the protocol above.

Statistical Analysis

Statistical analysis (with $P < 0.05$ considered significant) was performed with unpaired, two-tailed Student's *t*-test. Error bars indicate SEM. Asterisks indicate significance, $^{*}P \leq 0.05$, $^{**}P \leq 0.01$, $^{***}P \leq 0.001$.

RESULTS

Accumulation of Aβ Deposits in the Eyes of TgF344-AD Tg Rat

We first wanted to confirm that there was a buildup of Aβ in the brain and retina of the AD rats as shown previously for the AD mouse.[24–26] Immunofluorescent staining with anti-human Aβ plaque-specific antibody 6E10 showed no positive staining in the WT rat brain (Figs. 1A, 1B); in contrast, robust deposition of Aβ plaques with variable sizes in both hippocampus (Fig. 1C) and cortex (Fig. 1D) was detected in the TgF344-AD rat brain. Using the same antibody in the retina, no immunoreactivity was found in the WT retinas (Fig. 1E), whereas the senile plaque-like staining was found in the inner plexiform layer (IPL), outer plexiform layer (OPL), and choroid (Figs. 1F–H) of 19-month-old Tg rats. Only few amyloid plaques were observed in 14-month-old Tg rats. There was no positive signal detected (Supplementary Fig. S1) in negative controls (PBS to replace the primary antibody and/or the secondary antibody).

The same antibody was applied to human postmortem retinas from both AD patients and age-matched controls, with brain sections from Tg rat as positive control. Virtually no Aβ plaques were found in non-AD human retinal sections as revealed by anti-human Aβ plaque-specific antibody 6E10 staining of retinal whole mounts. Plaque-like structures (Supplementary Figs. S2A, S2B versus control C-without primary antibody) were found in two retinas from two AD patients, with denser morphology than those seen in Tg rat brain. Further analysis revealed that there were two and 27 plaque-like structures per retinal whole-mount in these two AD cases, which could reflect the disease severity. Thioflavin-T staining failed to detect positive staining in the other two retinas from these two AD patients. However, this result may have been influenced by standard acid treatment during Thioflavin-T staining.

Visual Function Is Impaired in the Rat Model of AD

We next established whether visual acuity of Tg rats was altered relative to aged-matched WT rats by testing OKR at age 19 months. Spatial frequency thresholds declined to approximately 0.15 cyc/deg in Tg rats, compared with 0.22 cyc/deg in WT rats (Fig. 2A), and this difference was significant ($P < 0.005$). Contrast sensitivity was increased in 19-month-old Tg rats (>50 %) compared with WT rats (15%–18%; preliminary observation on limited rats). This is an interesting observation. Further study is needed to confirm this difference. In order to examine whether retinal sensitivities to light stimuli are altered in AD eyes, luminance thresholds were also recorded in both WT and Tg rats (age 19 months). The thresholds were viable across the SC in both groups (Figs. 2B, 2C) from 0.1 to 0.6 and

Investigative Ophthalmology & Visual Science

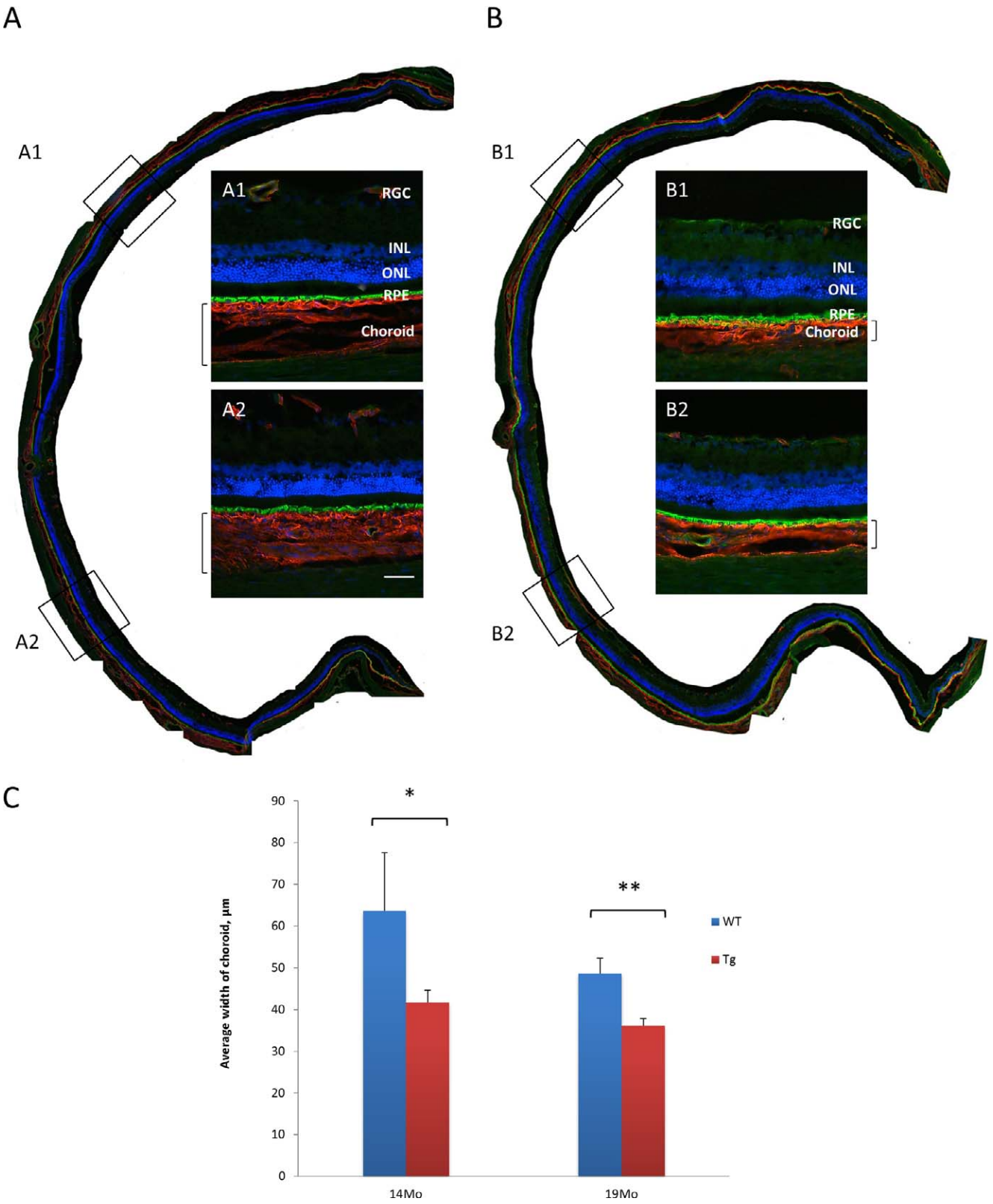

Figure 3. The retinal sections were double stained with antibodies against type IV collagen (*red*) and RPE65 (*green*) in WT (**A**) and Tg (**B**) rats. The *boxes* correspond to the high power images, which show obvious reduction in choroidal thickness in Tg (B1, B2) than in WT rats (A1, A2). Nuclei were counterstained with DAPI (*blue*). *Scale bars*: 50 µm. (**C**) Measurements of the choroidal thickness from 14- and 19-month-old Tg and age-matched WT rats revealed that there was significant difference between Tg and WT groups at both age groups. Mean ± SEM, $n = 5$. $^{*}P \leq 0.05$. $^{**}P \leq 0.01$ compared with WT rats of both ages.

Investigative Ophthalmology & Visual Science

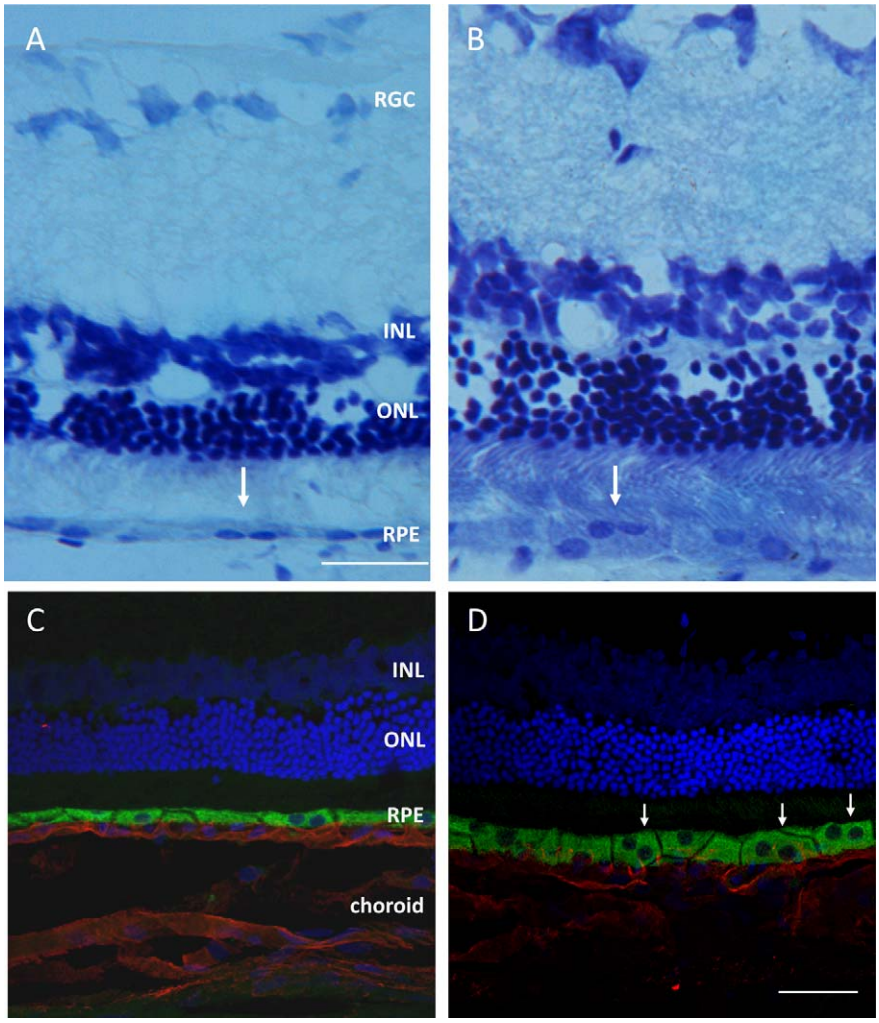

FIGURE 4. Histology of 19-month-old WT and TgF344-AD rats. Retinal sections obtained from 19-month-old WT (**A**, **C**) and Tg rats (**B**, **D**) were stained with cresyl violet (**A**, **B**) antibodies to RPE65 (*green*) and type IV collagen (*red*; [**C**, **D**]), and counterstained with DAPI (*blue*). The hypertrophic and multiple nuclei of RPE cells (*arrows* in [**B**, **D**]) were observed in Tg retina. *Scale bars*: 50 μm.

–0.1 to 0.5 log units in Tg rats and WT, respectively. Overall, there was no difference on the retinal sensitivities to light stimuli between Tg and WT rats.

Morphological Changes in the RPE Cells and Choroid of the AD Rat

Previous studies have shown abnormal inner retinal pathologies in various AD Tg mouse models.[24–26] No prior studies have reported changes in the outer retina. Ocular histopathology assessments of the TgF344-AD rats and age-matched WT rats in this study were performed at the age of 14 ($n = 6$) and 19 ($n = 5$) months. To assess the thickness of the choroid, the immunoreactivity of choroidal vessels was evaluated following basement membrane-specific antibody staining for type IV collagen. Overall, the thickness of the choroid was uneven across the retina; it was thinner in the peripheral part than in the central retina. Interestingly, at 19 months, the thickness of the choroid in Tg rats was significantly reduced to 36.13 ± 1.71 μm (Figs. 3A, 3C), compared with 48.6 ± 3.74 μm ($P < 0.01$) in age-matched WT rats (Figs. 3B, 3C). This change has already been detected at 14 months, with choroidal thickness of 41.7 ± 2.96 μm in Tg rats and 63.57 ± 14.01 μm in WT rats ($P < 0.05$; Fig. 3C).

The monolayer of RPE wrapping around the outer retina and forming part of the blood-retinal barrier is important for fine visual acuity, visual cycle, and homeostasis.[37] To assess the morphological changes of RPE, retinal sections were stained with cresyl violet (Figs. 4A, 4B) and the RPE-specific marker RPE65 (Figs. 4C, 4D). In 19-month-old WT rats, RPE cells were flat and had few double nucleated cells (Figs. 4A, 4C). By comparison, in Tg rats RPE cells showed hypertrophy, and cells with double nuclei were more frequently found (Figs. 4B, 4D). The changes in the RPE cells were not observed in the limited human retinas.

Changes in Eyes From Patients With Alzheimer's Disease

To determine whether a similar pattern of choroid thinning was present in human tissues, 12 human retinas (seven male, and five female) aged 63–95 years were analyzed. The mean choroidal thickness decreased from 122.36 ± 24.87 μm to 84.75 ± 4.35 μm with aging (Table 2) in control donors. The mean thickness in normal samples was 98.79 ± 7.00 μm and was reduced to 73.17 ± 8.92 μm in AD samples ($P < 0.05$; Table 2). Although the sample size is small, the results parallel those from rats, with thinning of choroid in AD retinas

Investigative Ophthalmology & Visual Science

Table 2. Choroidal Thickness in Human Postmortem Retinas

Age, y/Sex	Mean Chorodial Thickness, µm	Age, y/Sex	Mean Chorodial Thickness, µm
Ctl 64 F	122.36 ± 24.87	AD 63 M	91.57 ± 0.19
Ctl 76 M	94.34 ± 1.60	AD 64 F*	41.56 ± 0.05
Ctl 80 M	84.75 ± 4.35	AD 75 F	85.50 ± 3.96
Ctl 85 M	75.66 ± 6.39	AD 80 M	55.30 ± 2.59
Ctl 93 F	108.44 ± 3.75	AD 80 M	68.32 ± 5.34
Ctl 95 F	107.19 ± 5.36	AD 95 F	96.75 ± 1.10

Ctl, control; F, female; M, male.
* The patient had glaucoma.

compared with age-matched controls. With the same protocol as above, retinal sections from both age-matched controls (Supplementary Fig. S3A) and AD (Supplementary Fig. S3B) were stained with antibodies against RPE65 and type IV collagen. The multiple nuclei of RPE cells often observed in Tg rat were not seen in AD retinas (Supplementary Fig. S3).

Other Significant Changes in the Eyes of TgF344-AD Rats

One of the main features accompanying deposition of Aβ plaques in AD is an inflammatory response characterized by infiltration of microglia and activation of complement. Therefore, we examined the expression of Iba-I and CD68, general and activated microglia-specific markers, respectively, and performed quantitative analysis to evaluate the infiltration of microglia. Figures 5A through 5D shows representative pictures of Iba-I and CD68 immunoreactivity in WT and Tg rats. Similar to the infiltration of microglia in the inner retinas of AD mice,[24,38] significantly increased Iba-I immunoreactivity was detected in the choroid of Tg rats (Figs. 5B, 5E). In addition, activated microglia or neutrophils were also significantly increased in Tg rats based on CD68-positive signals (Figs. 5D, 5F). In the complement system, C3 is the key activator of the common and alternative pathways. Immunofluorescent labeling showed that C3 deposition along the Bruch's membrane was increased in Tg rats compared with age-matched WT rats (Figs. 5G, 5H).

Structural Observations in the Retina and Choroid of the AD Rat

To visualize the general retinal lamination, retinal sections were stained with cresyl violet. The uneven photoreceptor cell loss across the retina was observed in both aged WT and Tg rats (Figs. 6A, 6B). The photoreceptor loss was more prominent in the peripheral part of the retina with one to three layers of cells, whereas around the optic nerve head, the photoreceptors were about six to eight cells thick. The overall retinal lamination was still maintained in both WT and Tg rats. We did not detect the uneven loss of photoreceptors in AD retinas, although the inner nuclear layer (INL) seems to be much thinner (one to three layers) than in healthy controls (three to five layers, Supplementary Figs. S3A versus S3B). The reason for the thinning INL and any relation with pathology of AD needs further study.

Retinal blood flow studies have described a significant narrowing of the veins and reduced venous blood flow rate in AD patients.[16,39] The whole mount images of retinal vasculature labeled by type IV collagen antibody displayed a similar pattern of vascular structure between WT and Tg rats (Figs. 6C, 6E) and abnormal thinning of retinal vessels was not observed. In addition, retinal ganglion cell (RGC) loss was reported in AD patients.[11,40] However, we did not see obvious difference in the RGC numbers between WT and Tg eyes (Figs. 6D, 6F).

Upregulation of glial fibrillary acidic protein (GFAP) expression in the retinal Müller glial cells has been well documented in a variety of retinal insults including injury, diabetic retinopathy, aging, and degeneration.[41–43] In the WT rats at 19 months, there were active Müller glial cells as revealed by GFAP staining (Fig. 5I); while in TgF344-AD rats, the expression of GFAP in radial Müller glia was more evident than in WT animals (Figs. 5I, 5J).

Discussion

In the present study, we showed for the first time a marked thinning of retinal choroid and hypertrophic RPE in TgF344-AD rat, a novel rat model that manifests the spectrum of age-dependent AD pathologies.[27] The similar thinning of the choroid was also observed in a limited series of human postmortem specimens. Detection of Aβ plaques in the retinas and brains of Tg rats was confirmed by 6E10 antibody, which exhibited a similar staining pattern to a mouse model of AD.[24,44] Aβ deposition in the retina may explain the increase of inflammation, complement activation, and a decline of visual function in the Tg rats, although no apparent neuronal cell loss was observed in RGC based on neuronal tracer (Fluorochrome, LLC) labeling. One study has found Aβ plaques deposition in human retina,[45] and we have also seen plaque-like staining in two AD retinal whole mounts as revealed by anti-human Aβ plaque-specific antibody 6E10. Regardless of the mechanism of how Aβ becomes detrimental to the retina, our results highlight the pathological changes in the outer retina associated with AD.

Changes in Choroid and RPE Layer

The choroid is one of the most highly vascularized tissues of the body, provides oxygen and nourishment to the outer retina, modulates retinal temperature, secretes growth factors, and adjusts the retinal position. The choroid is involved in the pathogenesis of various ocular diseases[46] such as pathological myopia,[47,48] glaucoma,[49,50] diabetic retinopathy,[51,52] AMD,[53,54] and age-related choroidal atrophy.[55] In the case of type 2 diabetes, the decreased choroidal blood flow may occur before the clinical manifestations of diabetic retinopathy. In addition, the loss of choriocapillaris could increase vascular resistance, resulting in decreased blood flow. The observations of pathological variations in choroidal thickness suggested that the choroidal thickness could be an important parameter in the evaluation of ocular and other diseases. Interestingly, numerous structural and functional cerebral microvascular abnormalities have been identified since microvascular perturbations have been highlighted in AD over 25 years ago.[56] The topographic associations of capillaries and neuritic plaques are highly correlated,[57] and abnormalities of blood vessels are evident before the formation of parenchymal amyloid plaques in a Tg mouse model of AD.[58] Indeed, robust microvascular Aβ deposition in the retina of Tg mice was well documented in the line Tg2567.[26] From these studies, we hypothesize that the changes in the retinal choroid and Aβ deposition in the retina could be relevant to the pathologies observed in the brain. On the other hand, not only ocular diseases but also aging causes the decrease of choroidal thickness, which has been documented in several studies.[32,59–61] Although the choroidal changes are small relative to other severe symptoms, they may play an important role in the visual regulation and eventually affect visual function.[62,63]

Investigative Ophthalmology & Visual Science

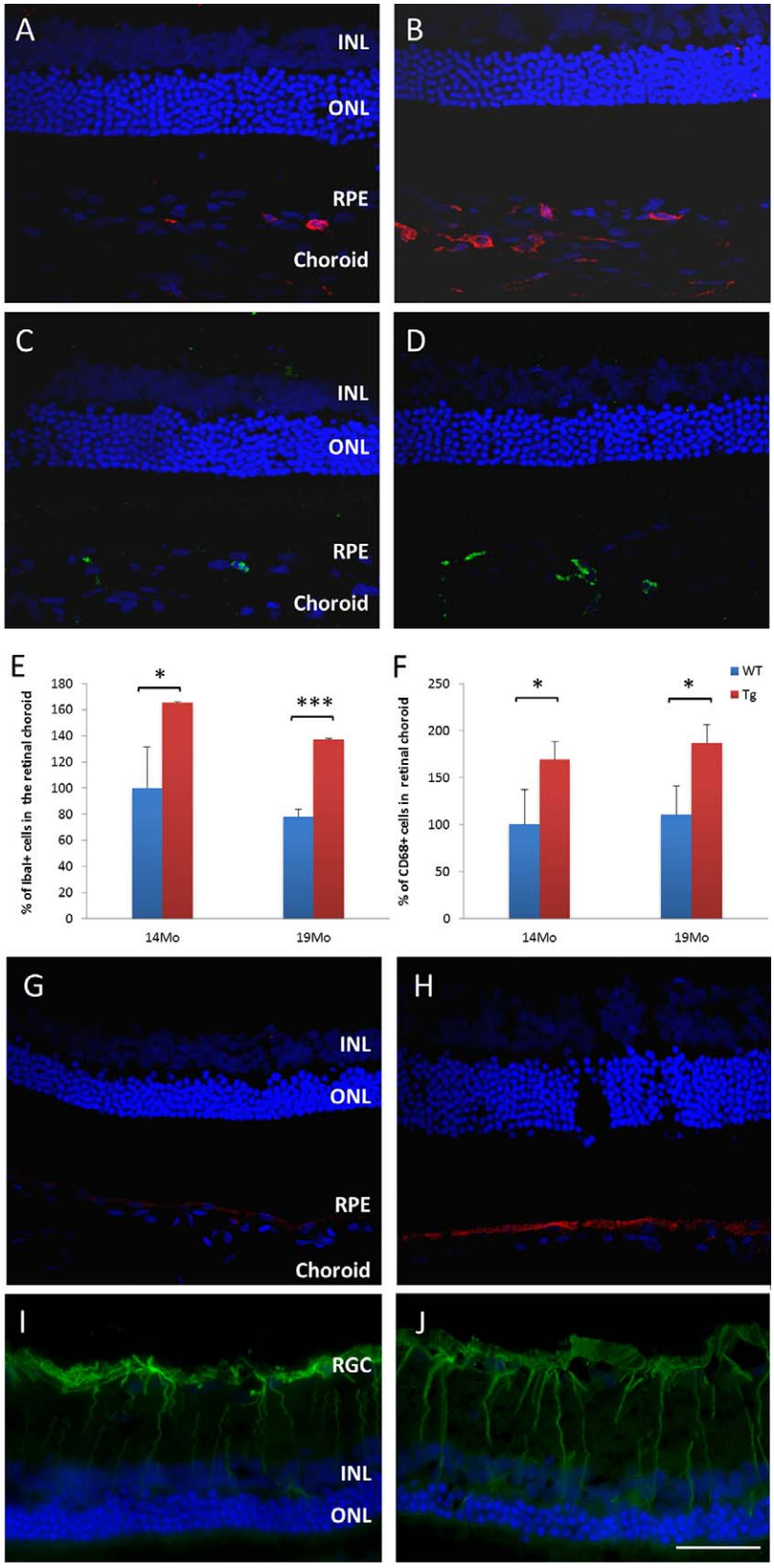

Figure 5. Infiltration of inflammatory cells and activation of C3 complement in 19-month-old Tg rats. Retinal sections were stained for Iba-1 (*red*; [**A**], [**B**]) and CD68 (*green*; [**C**, **D**]). An increase of Iba-1 and CD68 signal was observed in Tg rats (**B**, **D**). Quantification of the Iba-1 (**E**) and CD68 (**F**) positive cells in the choroid of 14- and 19-month-old Tg and age-matched WT rats revealed significant differences between Tg and WT rats in both age groups (mean ± SEM, $n = 4$. $^{*}P \leq 0.05$. $^{***}P \leq 0.001$). Retinal sections stained with antibody against C3 (*red*) and counterstained with DAPI (*blue*) showed an activated C3 complement signal along the RPE layer in Tg rat (**H**) compared with WT control (**G**). GFAP staining showed more obvious upregulation of the protein expression in radial Müller glia in Tg rat (**J**) compared with WT control (**I**). *Scale bars*: 50 μm.

Investigative Ophthalmology & Visual Science

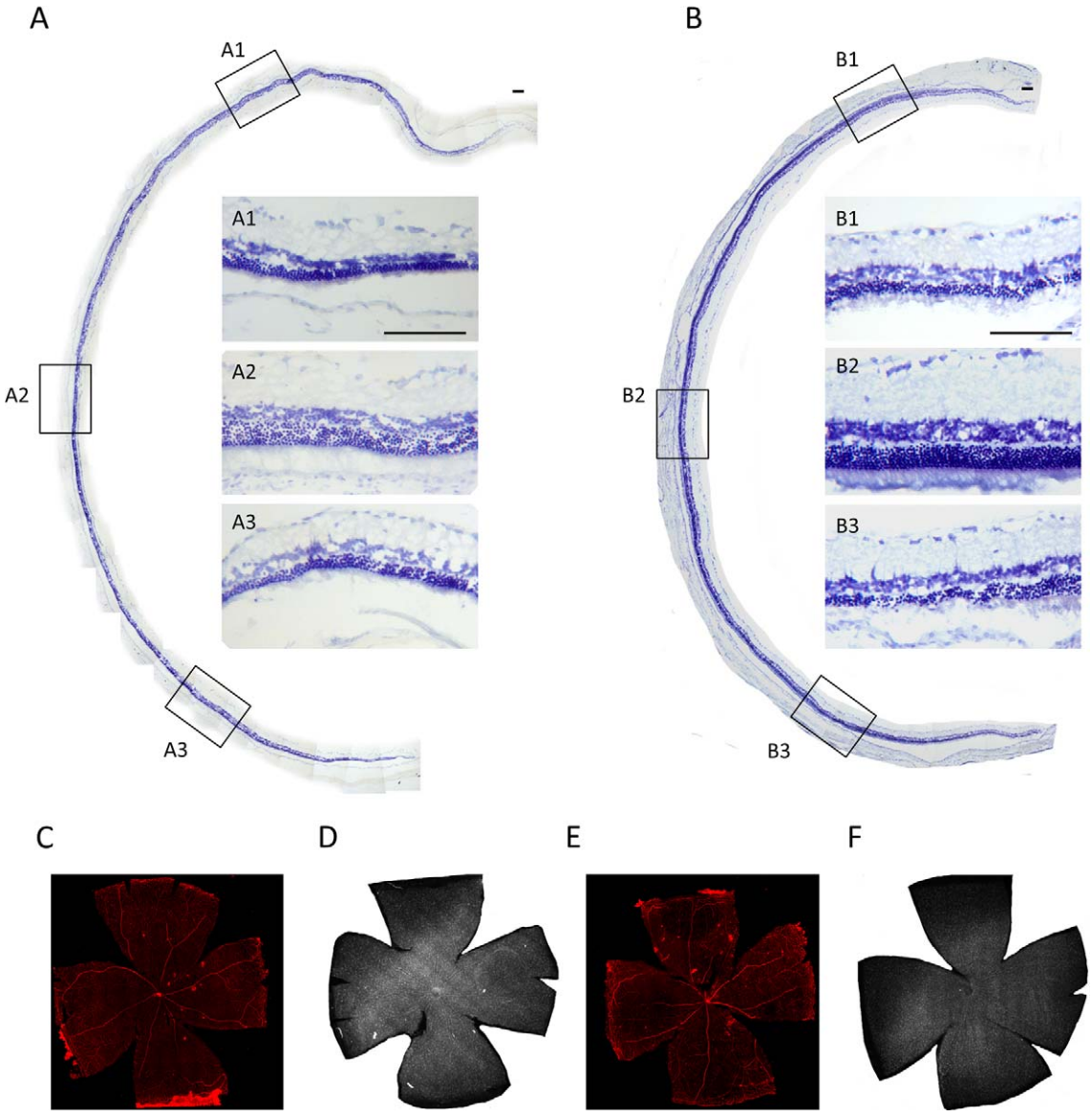

Figure 6. Cresyl violet stained retinal sections from WT (**A**) and Tg (**B**) rats. Note that the thickness of the ONL was uneven across the retina: two to three layers in the peripheral parts and six to eight cells thick in the central part of the retina. A1 through A3 and B1 through B3 are high-power images of the corresponding outlined areas. *Scale bars*: 100 μm. The profiles of retinal blood vessels were visualized by antibody against type IV collagen in WT (**C**) and Tg (**E**) rats in retinal whole mount preparation. There was no obvious difference between WT and Tg rats. RGCs were retrogradely labeled with neuronal tracer (Fluorochrome, LLC; 5 days after applying the neuronal tracer [Fluorochrome, LLC] into the SC). Retinal whole mounts showed no obvious difference between WT (**D**) and Tg (**F**) rats in the density of RGC. *Scale bars*: 100 μm.

RPE cell dysfunction is relevant to various retinal degenerative diseases, which illustrates the importance of the RPE for photoreceptor viability. RPE hypertrophy is a cardinal feature of the stress response triggered by various perturbations, such as iron accumulation[64–66] and oxidative damage.[67] Interestingly, injection of oligomeric Aβ peptide into the subretinal space of B6 mice induces RPE hypertrophy and pigmentation loss but not apoptosis, which supports the idea of oxidative stress involvement in the alterations of RPE function.[68] Although aging also leads to abnormal RPE function, we found more frequent RPE hypertrophy in 14 and 19 months TgF344-AD rats compared with age-matched WT control rats (Fig. 4), which underline the effect of Aβ on RPE dysfunction. Furthermore, RPE hypertrophy has also been described in advanced AMD in humans[69,70] and may occur earlier in the progress of the disease. Thus, the morphological and functional changes in RPE cells are likely to be a characteristic of ocular and neurodegenerative disease.

Visual Acuity and Inner Retinal Changes

Visual acuity varies with different strains in animal models.[71] Indeed, the Fischer-344 rats with albinism showed poorer visual acuity than pigmented rats.[28,30] In the TgF344-AD rats, visual acuity was lower than in age-matched WT rats (Fig. 2). However, the fundamental mechanisms underlying the Aβ pathology association with visual acuity need further studies. The thinning choroid may contribute the poor visual performance as well. Morphologically, we saw uneven loss of photoreceptors across the retina, which correlated with the data from luminance threshold recording. Although the luminance thresholds were elevated in both Tg and WT rats

compared with pigmented WT rats,[28] there are compensatory mechanisms within retinal circuitry and the superior colliculus since the retinal responses to light stimulation are still rather sensitive. We did not observe the uneven loss of photoreceptors in human AD retinas, which indicates the limitation of this rat model. Although AD transgenic animal models show similarities across various studies,[72] variations of the onset of the amyloid plaque formation and retinal changes in different lines are presumably explained by differences in animal strains, promoters, and specific mutations used. Also, animal models may not faithfully recapitulate the pathology of human patients. The RGC loss has been described in AD patients[10,11] and in some animal models of AD.[26,45] In TgF344-AD rats, no obvious changes in the RGC numbers compared with age-matched WT rats were observed. This result is in agreement with data from APPswe/PS1ΔE9 Tg mouse study, which showed the absence of significant neuronal loss.[24] Again, the current rat and mouse models for AD do not appear to recapitulate the full pathology of human patients. Recent reports suggested that RGC dendritic atrophy may precede cell loss,[73,74] calling for further studies to examine the morphology of RGC.

Immunological Responses

A role for inflammation in the pathogenesis of AD is suggested by the presence of activated microglia[75,76] and proinflammatory cytokines, chemokines, and complement proteins[77,78] in the brain of AD patients, which are not evident in the normal brain. Microglia have been found to be preferentially associated with certain amyloid plaque types.[79] Once microglial cells are activated, the secretion of inflammatory cytokines, such as TNF-α and IL-1β,[80] contributes to Aβ deposition and the early pathogenic changes in AD.[81] Nevertheless, activated microglia can also be beneficial by phagocytosis of Aβ[82] and secretion of anti-inflammatory factors. The activation of complement system involved in neuronal death at the early stages of AD has also been reported in human and Tg animal studies.[83–86] Notably, we observed the recruitment of microglia and the activation of complement protein C (Fig. 5) in the choroid suggesting an inflammatory response in the ocular vascular system. Although the main causes and progression of the inflammatory response in the AD eye are still unclear, it is possible that chronic ocular inflammation early in life may set the stage later for the development of AD.

Implications

In the clinical application, the optical coherence tomography (OCT) provides a noninvasive, noncontact, transpupillary imaging modality to monitor retinal changes. Since the introduction of enhanced depth imaging based on OCT (EDI-OCT) technology by Spaide,[87] changes in choroidal vasculature and volume have been reported in chorioretinal disorders accurately and reproducibly.[54,88–90] In humans, some studies have indicated that choroidal thickness is dynamic and influenced by the time of the day,[91,92] retinal location,[59] and age.[32,60] Accordingly, for the future diagnostic purpose, the above factors should be considered.

In summary, we have observed pathological changes in the choroid and RPE cells in TgF344-AD rat model, and the same choroidal thinning in a limited number of human AD retinas. Along with Aβ deposition, the inflammatory response manifested by microglial recruitment and complement activation was seen in the choroid. Further study is needed to investigate the mechanisms of these ocular changes and their relation with changes in the brain. The long-term goal will be to aid early diagnosis of AD by studying the eye, the approachable part of the brain.

Acknowledgments

The authors thank Terrence Town, PhD, and Tara M. Weitz, PhD (University of Southern California, Keck School of Medicine, Los Angeles, CA) for sharing tissue from 14-month-old AD rats. We thank Claudia Tan and Mary Bessell for proofreading this manuscript, and Carol Church and Jeanette Espinosa for their administrative support at the Alzheimer's Disease Research Center at the University of Southern California.

Supported by Grants NIH R01 EY020488-02, W81XWH-DOD, the Lincy Foundation, FFB, the Fund from the Regenerative Medicine Institute at Cedars-Sinai Medical Center, the National Institute of Aging Grant P50-AG05142, and NIH R01 EY03040 (FNR-C and AAS).

Disclosure: **Y. Tsai**, None; **B. Lu**, None; **A.V. Ljubimov**, None; **S. Girman**, None; **F.N. Ross-Cisneros**, None; **A.A. Sadun**, None; **C.N. Svendsen**, None; **R.M. Cohen**, None; **S. Wang**, None

References

1. Batsch NL, Mittelman MS, eds. *World Alzheimer Report 2012: Overcoming the Stigma of Dementia*. London: Alzheimer's Disease International; 2012:75.
2. Holtzman DM, Morris JC, Goate AM. Alzheimer's disease: the challenge of the second century. *Sci Transl Med*. 2011;3:77sr1.
3. Katz B, Rimmer S. Ophthalmologic manifestations of Alzheimer's disease. *Surv Ophthalmol*. 1989;34:31–43.
4. Uhlmann RF, Larson EB, Koepsell TD, Rees TS, Duckert LG. Visual impairment and cognitive dysfunction in Alzheimer's disease. *J Gen Intern Med*. 1991;6:126–132.
5. Cronin-Golomb A, Corkin S, Rizzo JF, Cohen J, Growdon JH, Banks KS. Visual dysfunction in Alzheimer's disease: relation to normal aging. *Ann Neurol*. 1991;29:41–52.
6. Pache M, Smeets CH, Gasio PF, et al. Colour vision deficiencies in Alzheimer's disease. *Age Ageing*. 2003;32:422–426.
7. Gilmore GC, Wenk HE, Naylor LA, Koss E. Motion perception and Alzheimer's disease. *J Gerontol*. 1994;49:P52–P57.
8. Armstrong RA. Visual field defects in Alzheimer's disease patients may reflect differential pathology in the primary visual cortex. *Optom Vis Sci*. 1996;73:677–682.
9. Trick GL, Trick LR, Morris P, Wolf M. Visual field loss in senile dementia of the Alzheimer's type. *Neurology*. 1995;45:68–74.
10. Blanks JC, Hinton DR, Sadun AA, Miller CA. Retinal ganglion cell degeneration in Alzheimer's disease. *Brain Res*. 1989;501:364–372.
11. Blanks JC, Torigoe Y, Hinton DR, Blanks RH. Retinal pathology in Alzheimer's disease. I. Ganglion cell loss in foveal/parafoveal retina. *Neurobiol Aging*. 1996;17:377–384.
12. Hinton DR, Sadun AA, Blanks JC, Miller CA. Optic-nerve degeneration in Alzheimer's disease. *N Engl J Med*. 1986;315:485–487.
13. Hedges TR, Perez Galves R, Speigelman D, Barbas NR, Peli E, Yardley CJ. Retinal nerve fiber layer abnormalities in Alzheimer's disease. *Acta Ophthalmol Scand*. 1996;74:271–275.
14. Kesler A, Vakhapova V, Korczyn AD, Naftaliev E, Neudorfer M. Retinal thickness in patients with mild cognitive impairment and Alzheimer's disease. *Clin Neurol Neurosurg*. 2011;113:523–526.
15. Sadun AA, Bassi CJ. Optic nerve damage in Alzheimer's disease. *Ophthalmology*. 1990;97:9–17.
16. Berisha F, Feke GT, Trempe CL, McMeel JW, Schepens CL. Retinal abnormalities in early Alzheimer's disease. *Invest Ophthalmol Vis Sci*. 2007;48:2285–2289.
17. Sadun AA, Borchert M, DeVita E, Hinton DR, Bassi CJ. Assessment of visual impairment in patients with Alzheimer's disease. *Am J Ophthalmol*. 1987;104:113–120.

18. London A, Benhar I, Schwartz M. The retina as a window to the brain-from eye research to CNS disorders. *Nat Rev Neurol*. 2013;9:44–53.
19. Tanzi RE, Moir RD, Wagner SL. Clearance of Alzheimer's Aβ peptide: the many roads to perdition. *Neuron*. 2004;43:605–608.
20. Zlokovic BV. Clearing amyloid through the blood-brain barrier. *J Neurochem*. 2004;89:807–811.
21. Chalbot S, Zetterberg H, Blennow K, et al. Blood-cerebrospinal fluid barrier permeability in Alzheimer's disease. *J Alzheimers Dis*. 2011;25:505–515.
22. Zlokovic BV, Martel CL, Matsubara E, et al. Glycoprotein 330/megalin: probable role in receptor-mediated transport of apolipoprotein J alone and in a complex with Alzheimer disease amyloid beta at the blood-brain and blood-cerebrospinal fluid barriers. *Proc Natl Acad Sci U S A*. 1996;93:4229–4234.
23. Braidy N, Muñoz P, Palacios AG, et al. Recent rodent models for Alzheimer's disease: clinical implications and basic research. *J Neural Transm*. 2012;119:173–195.
24. Perez SE, Lumayag S, Kovacs B, Mufson EJ, Xu S. Beta-amyloid deposition and functional impairment in the retina of the APPswe/PS1DeltaE9 transgenic mouse model of Alzheimer's disease. *Invest Ophthalmol Vis Sci*. 2009;50:793–800.
25. Liu B, Rasool S, Yang Z, et al. Amyloid-peptide vaccinations reduce beta-amyloid plaques but exacerbate vascular deposition and inflammation in the retina of Alzheimer's transgenic mice. *Am J Pathol*. 2009;175:2099–2110.
26. Ning A, Cui J, To E, Ashe KH, Matsubara J. Amyloid-β deposits lead to retinal degeneration in a mouse model of Alzheimer disease. *Invest Ophthalmol Vis Sci*. 2008;49:5136–5143.
27. Cohen RM, Rezai-Zadeh K, Weitz TM, et al. A Transgenic Alzheimer rat with plaques, tau pathology, behavioral impairment, oligomeric Aβ, and frank neuronal loss. *J Neurosci*. 2013;33:6245–6256.
28. Lu B, Morgans CW, Girman S, et al. Neural stem cells derived by small molecules preserve vision. *Transl Vis Sci Technol*. 2013;2:1.
29. Girman SV, Lund RD. Most superficial sublamina of rat superior colliculus: neuronal response properties and correlates with perceptual figure-ground segregation. *J Neurophysiol*. 2007;98:161–177.
30. Wang S, Lu B, Girman S, et al. Non-invasive stem cell therapy in a rat model for retinal degeneration and vascular pathology. *PLoS One*. 2010;5:e9200.
31. Jehle T, Wingert K, Dimitriu C, et al. Quantification of ischemic damage in the rat retina: a comparative study using evoked potentials, electroretinography, and histology. *Invest Ophthalmol Vis Sci*. 2008;49:1056–1064.
32. Ramrattan RS, van der Schaft TL, Mooy CM, de Bruijn WC, Mulder PG, de Jong PT. Morphometric analysis of Bruch's membrane, the choriocapillaris, and the choroid in aging. *Invest Ophthalmol Vis Sci*. 1994;35:2857–2864.
33. Grieshaber P, Lagrèze WA, Noack C, Boehringer D, Biermann J. Staining of Fluorogold-prelabeled retinal ganglion cells with calcein-AM: a new method for assessing cell vitality. *J Neurosci Methods*. 2010;192:233–239.
34. Braak H, Alafuzoff I, Arzberger T, Kretzschmar H, Del Tredici K. Staging of Alzheimer disease-associated neurofibrillary pathology using paraffin sections and immunocytochemistry. *Acta Neuropathol*. 2006;112:389–404.
35. Mirra SS, Heyman A, McKeel D, et al. The Consortium to Establish a Registry for Alzheimer's Disease (CERAD). Part II. Standardization of the neuropathologic assessment of Alzheimer's disease. *Neurology*. 1991;41:479–486.
36. Thioflavin T stain: an easier and more sensitive method for amyloid detection. In Picken MM, Herrera GA, eds. *Amyloid and Related Disorders: Surgical Pathology and Clinical Correlations*. New York: Humana Press; 2012:187–189.
37. Simó R, Villarroel M, Corraliza L, Hernández C, Garcia-Ramírez M. The retinal pigment epithelium: something more than a constituent of the blood-retinal barrier–implications for the pathogenesis of diabetic retinopathy. *J Biomed Biotechnol*. 2010;2010:190724.
38. Liu B, Rasool S, Yang Z, et al. Amyloid-peptide vaccinations reduce β-amyloid plaques but exacerbate vascular deposition and inflammation in the retina of Alzheimer's transgenic mice. *Am J Pathol*. 2009;175:2099–2110.
39. Iseri PK, Altinaş O, Tokay T, Yüksel N. Relationship between cognitive impairment and retinal morphological and visual functional abnormalities in Alzheimer disease. *J Neuroophthalmol*. 2006;26:18–24.
40. Blanks JC, Schmidt SY, Torigoe Y, Porrello KV, Hinton DR, Blanks RH. Retinal pathology in Alzheimer's disease. II. Regional neuron loss and glial changes in GCL. *Neurobiol Aging*. 1996;17:385–395.
41. Roque RS, Caldwell RB. Müller cell changes precede vascularization of the pigment epithelium in the dystrophic rat retina. *Glia*. 1990;3:464–475.
42. DiLoreto DA, Martzen MR, del Cerro C, Coleman PD, del Cerro M. Müller cell changes precede photoreceptor cell degeneration in the age-related retinal degeneration of the Fischer 344 rat. *Brain Res*. 1995;698:1–14.
43. Tanihara H, Hangai M, Sawaguchi S, et al. Up-regulation of glial fibrillary acidic protein in the retina of primate eyes with experimental glaucoma. *Arch Ophthalmol*. 1997;115:752–756.
44. Borchelt DR, Ratovitski T, van Lare J, et al. Accelerated amyloid deposition in the brains of transgenic mice coexpressing mutant presenilin 1 and amyloid precursor proteins. *Neuron*. 1997;19:939–945.
45. Koronyo-Hamaoui M, Koronyo Y, Ljubimov AV, et al. Identification of amyloid plaques in retinas from Alzheimer's patients and noninvasive in vivo optical imaging of retinal plaques in a mouse model. *Neuroimage*. 2011;54(suppl 1):S204–S217.
46. Kur J, Newman EA, Chan-Ling T. Cellular and physiological mechanisms underlying blood flow regulation in the retina and choroid in health and disease. *Prog Retin Eye Res*. 2012;31:377–406.
47. Vincent SJ, Collins MJ, Read SA, Carney LG. Retinal and choroidal thickness in myopic anisometropia. *Invest Ophthalmol Vis Sci*. 2013;54:2445–2456.
48. Fujiwara T, Imamura Y, Margolis R, Slakter JS, Spaide RF. Enhanced depth imaging optical coherence tomography of the choroid in highly myopic eyes. *Am J Ophthalmol*. 2009;148:445–450.
49. Yin ZQ, Vaegan, Millar TJ, Beaumont P, Sarks S. Widespread choroidal insufficiency in primary open-angle glaucoma. *J Glaucoma*. 1997;6:23–32.
50. Usui S, Ikuno Y, Miki A, Matsushita K, Yasuno Y, Nishida K. Evaluation of the choroidal thickness using high-penetration optical coherence tomography with long wavelength in highly myopic normal-tension glaucoma. *Am J Ophthalmol*. 2012;153:10–16.e11.
51. Querques G, Lattanzio R, Querques L, et al. Enhanced depth imaging optical coherence tomography in type 2 diabetes. *Invest Ophthalmol Vis Sci*. 2012;53:6017–6024.
52. Esmaeelpour M, Brunner S, Ansari-Shahrezaei S, et al. Choroidal thinning in diabetes type 1 detected by 3-dimensional 1060 nm optical coherence tomography. *Invest Ophthalmol Vis Sci*. 2012;53:6803–6809.
53. Kim JH, Kim JR. Kang Se W, Kim SJ, Ha HS. Thinner choroid and greater Drusen extent in retinal angiomatous proliferation than in typical exudative age-related macular degeneration. *Am J Ophthalmol*. 2013;155:743–749.e742.
54. Jirarattanasopa P, Ooto S, Nakata I, et al. Choroidal thickness, vascular hyperpermeability, and complement factor H in age-

Investigative Ophthalmology & Visual Science

related macular degeneration and polypoidal choroidal vasculopathy. *Invest Ophthalmol Vis Sci*. 2012;53:3663–3672.

55. Spaide RF. Age-related choroidal atrophy. *Am J Ophthalmol*. 2009;147:801–810.
56. Scheibel AB. Changes in brain capillary structure in aging and dementia. In: Wertheimer J, Marois M, eds. *Senile Dementia Outlook for the Future*. New York: Alan R. Liss, Inc.; 1984: 137–149.
57. Miyakawa T, Shimoji A, Kuramoto R, Higuchi Y. The relationship between senile plaques and cerebral blood vessels in Alzheimer's disease and senile dementia. Morphological mechanism of senile plaque production. *Virchows Arch B Cell Pathol Incl Mol Pathol*. 1982;40:121–129.
58. Meyer EP, Ulmann-Schuler A, Staufenbiel M, Krucker T. Altered morphology and 3D architecture of brain vasculature in a mouse model for Alzheimer's disease. *Proc Natl Acad Sci U S A*. 2008;105:3587–3592.
59. Margolis R, Spaide RF. A pilot study of enhanced depth imaging optical coherence tomography of the choroid in normal eyes. *Am J Ophthalmol*. 2009;147:811–815.
60. Manjunath V, Taha M, Fujimoto JG, Duker JS. Choroidal thickness in normal eyes measured using Cirrus HD optical coherence tomography. *Am J Ophthalmol*. 2010;150:325–329.e321.
61. Ding X, Li J, Zeng J, et al. Choroidal thickness in healthy Chinese subjects. *Invest Ophthalmol Vis Sci*. 2011;52:9555–9560.
62. Ayton LN, Guymer RH, Luu CD. Choroidal thickness profiles in retinitis pigmentosa. *Clin Experiment Ophthalmol*. 2013;41: 396–403.
63. Wang N-K, Lai C-C, Chou CL, et al. Choroidal thickness and biometric markers for the screening of lacquer cracks in patients with high myopia. *PLoS One*. 2013;8:e53660.
64. Gnana-Prakasam JP, Thangaraju M, Liu K, et al. Absence of iron-regulatory protein Hfe results in hyperproliferation of retinal pigment epithelium: role of cystine/glutamate exchanger. *Biochem J*. 2009;424:243–252.
65. Hadziahmetovic M, Dentchev T, Song Y, et al. Ceruloplasmin/hephaestin knockout mice model morphologic and molecular features of AMD. *Invest Ophthalmol Vis Sci*. 2008;49:2728–2736.
66. Chen H, Lukas TJ, Du N, Suyeoka G, Neufeld AH. Dysfunction of the retinal pigment epithelium with age: increased iron decreases phagocytosis and lysosomal activity. *Invest Ophthalmol Vis Sci*. 2009;50:1895–1902.
67. Zhao C, Yasumura D, Li X, et al. mTOR-mediated dedifferentiation of the retinal pigment epithelium initiates photoreceptor degeneration in mice. *J Clin Invest*. 2011;121:369–383.
68. Bruban J, Glotin AL, Dinet V, et al. Amyloid-β(1-42) alters structure and function of retinal pigmented epithelial cells. *Aging Cell*. 2009;8:162–177.
69. Coleman HR, Chan CC, Ferris FL, Chew EY. Age-related macular degeneration. *Lancet*. 2008;372:1835–1845.
70. De S, Rabin DM, Salero E, Lederman PL, Temple S, Stern JH. Human retinal pigment epithelium cell changes and expression of αB-crystallin: a biomarker for retinal pigment epithelium cell change in age-related macular degeneration. *Arch Ophthalmol*. 2007;125:641–645.
71. Prusky GT, Harker KT, Douglas RM, Whishaw IQ. Variation in visual acuity within pigmented, and between pigmented and albino rat strains. *Behav Brain Res*. 2002;136:339–348.
72. Elder GA, Gama Sosa MA, De Gasperi R. Transgenic mouse models of Alzheimer's disease. *Mt Sinai J Med*. 2010;77:69–81.
73. Damiani D, Novelli E, Mazzoni F, Strettoi E. Undersized dendritic arborizations in retinal ganglion cells of the rd1 mutant mouse: a paradigm of early onset photoreceptor degeneration. *J Comp Neurol*. 2012;520:1406–1423.
74. Williams PA, Thirgood RA, Oliphant H, et al. Retinal ganglion cell dendritic degeneration in a mouse model of Alzheimer's disease. *Neurobiol Aging*. 2013;34:1799–1806.
75. Cagnin A, Brooks DJ, Kennedy AM, et al. In-vivo measurement of activated microglia in dementia. *Lancet*. 2001;358:461–467.
76. Okello A, Edison P, Archer HA, et al. Microglial activation and amyloid deposition in mild cognitive impairment: a PET study. *Neurology*. 2009;72:56–62.
77. Cacquevel M, Lebeurrier N, Chéenne S, Vivien D. Cytokines in neuroinflammation and Alzheimer's disease. *Curr Drug Targets*. 2004;5:529–534.
78. Wyss-Coray T. Inflammation in Alzheimer disease: driving force, bystander or beneficial response? *Nat Med*. 2006;12: 1005–1015.
79. D'Andrea MR, Cole GM, Ard MD. The microglial phagocytic role with specific plaque types in the Alzheimer disease brain. *Neurobiol Aging*. 2004;25:675–683.
80. Liao Y-F, Wang B-J, Cheng H-T, Kuo L-H, Wolfe MS. Tumor necrosis factor-α, interleukin-1β, and interferon-γ stimulate γ-secretase-mediated cleavage of amyloid precursor protein through a JNK-dependent MAPK pathway. *J Biol Chem*. 2004;279:49523–49532.
81. Glass CK, Saijo K, Winner B, Marchetto MC, Gage FH. Mechanisms underlying inflammation in neurodegeneration. *Cell*. 2010;140:918–934.
82. Weldon DT, Rogers SD, Ghilardi JR, et al. Fibrillar β-amyloid induces microglial phagocytosis, expression of inducible nitric oxide synthase, and loss of a select population of neurons in the rat CNS in vivo. *J Neurosci*. 1998;18:2161–2173.
83. Eikelenboom P, Hack CE, Rozemuller JM, Stam FC. Complement activation in amyloid plaques in Alzheimer's dementia. *Virchows Arch B Cell Pathol Incl Mol Pathol*. 1989;56:259–262.
84. Loeffler DA, Camp DM, Bennett DA. Plaque complement activation and cognitive loss in Alzheimer's disease. *J Neuroinflammation*. 2008;5:9.
85. Rogers J, Cooper NR, Webster S, et al. Complement activation by β-amyloid in Alzheimer disease. *Proc Natl Acad Sci U S A*. 1992;89:10016–10020.
86. Fonseca MI, Chu SH, Berci AM, et al. Contribution of complement activation pathways to neuropathology differs among mouse models of Alzheimer's disease. *J Neuroinflammation*. 2011;8:4.
87. Spaide RF, Koizumi H, Pozzoni MC, Pozonni MC. Enhanced depth imaging spectral-domain optical coherence tomography. *Am J Ophthalmol*. 2008;146:496–500.
88. Dhoot DS, Huo S, Yuan A, et al. Evaluation of choroidal thickness in retinitis pigmentosa using enhanced depth imaging optical coherence tomography. *Br J Ophthalmol*. 2013;97:66–69.
89. Sim DA, Keane PA, Mehta H, et al. Repeatability and reproducibility of choroidal vessel layer measurements in diabetic retinopathy using enhanced depth optical coherence tomography. *Invest Ophthalmol Vis Sci*. 2013;54:2893–2901.
90. Querques G, Lattanzio R, Querques L, et al. Enhanced depth imaging optical coherence tomography in type 2 diabetes. *Invest Ophthalmol Vis Sci*. 2012;53:6017–6024.
91. Tan CS, Ouyang Y, Ruiz H, Sadda SR. Diurnal variation of choroidal thickness in normal, healthy subjects measured by spectral domain optical coherence tomography. *Invest Ophthalmol Vis Sci*. 2012;53:261–266.
92. Chakraborty R, Read SA, Collins MJ. Diurnal variations in axial length, choroidal thickness, intraocular pressure, and ocular biometrics. *Invest Ophthalmol Vis Sci*. 2011;52:5121–5129.
93. Wisdom BJ, Gunwar S, Hudson MD, Noelken ME, Hudson BG. Type IV collagen of Engelbreth-Holm-Swarm tumor matrix: identification of constituent chains. *Connect Tissue Res*. 1992; 27:225–234.
94. Chen L, Miyamura N, Ninomiya Y, Handa JT. Distribution of the collagen IV isoforms in human Bruch's membrane. *Br J Ophthalmol*. 2003;87:212–215.

Investigative Ophthalmology & Visual Science